DOI: https://doi.org/10.54966/jreen.v1i1.1266

Journal of Renewable Energies

Revue des Energies Renouvelables

journal home page: https://revue.cder.dz/index.php/rer

Conference paper

Heat transfer enhancement in a large-scale Ti-Mn based metal hydride storage reactor with nanofluids using open source CFD software

Allal Babou [a,b,*], **Yasmina Kerboua Ziari** [b], **Bachir Dadda** [a], **Toufik Chergui** [a], **Youcef Kerkoub** [b], **Oumaima Brakni** [b]

[a] *Unité de Recherche Appliquée en Energies Renouvelables, URAER, Centre de Développement des Energies Renouvelables, CDER, 47133, Ghardaïa, Algeria*

[b] *Laboratory of Thermodynamics and Energy Systems, Faculty of Physics, University of Science and Technology Houari Boumediene (USTHB), BP 32 El-Alia, Algiers, Algeria*

ARTICLE INFO

Article history:

Received August 1st, 2024

Accepted September 4, 2024

Keywords:

Hydrogen storage,
Heat and mass transfer,
Nanofluid,
OpenFOAM.

ABSTRACT

Metals can safely store hydrogen with high energy densities in the form of metal hydrides through an exothermic process. However, the slow hydrogen absorption kinetics significantly decreases its storage rate. Ensuring efficient heat dissipation from the metal hydride bed can result in a faster charging rate, which in turn improves the storage performance. The objective of this work is to improve the rate of heat and mass transfer in a Ti-Mn-based metal hydrides reactor for large-scale applications using a 3D model. Finite volume simulations with OpenFOAM software were conducted to investigate the influence of various parameters on the hydride reactors' performance. Water-based alumina (Al_2O_3/H_2O) nanofluid with varying volume fractions up to 5% are used as heat transfer fluids. The results show that accelerating the coolant flow velocity, decreasing its inlet temperature, and increasing the hydrogen supply pressure contribute further to enhancing thermal performance. Compared to pure water, the Al_2O_3/H_2O nanofluid with 5 vol % can improve heat transfer by approximately 11.5%. This can reduce the time needed to reach 90% storage by 18.1%. Also, the pressure drop throughout the hydride reactor at different flow velocities is slightly greater than that in pure water.

1. INTRODUCTION

The intense demand for non-renewable energy resources such as coal and petroleum inevitably causes an energy shortage, as well as serious environmental pollution caused by their use (Suranovic, 2013).

* *Corresponding author, E-mail address: a.babou@cder.dz*

ISSN: 1112-2242 / EISSN: 2716-8247

Therefore, there is an urgent need to switch to clean and durable energy resources. Among all types of renewable energies, hydrogen is gaining traction as a major player in the energy transition, with the highest energy content per unit weight compared to conventional fuels, making it a promising fuel for future applications (Mazzucco et al., 2014). Hydrogen is a clean fuel; it can produce green power when used as a fuel in combustion engines (Verhelst et al., 2014) or in fuel cells (Peighambardoust et al., 2010). The only exhaust gas is water vapor, which is environmentally friendly. Furthermore, various feedstock sources can produce it, including renewable energy sources like water splitting with wind (Taipabu et al., 2022), solar electricity (Ahmad et al., 2015), biogas reforming (Tanksale et al., 2010), and conventional energy sources like methane reforming or coal gasification (Msheik et al., 2021). Despite its high gravimetric energy density (143 MJ/kg (Demirel Y et al., 2012)), hydrogen has a low volumetric energy density at moderate conditions, making its storage a challenge. There are three common ways to store hydrogen gas: gaseous hydrogen storage under high pressure (about 70 MPa), liquid hydrogen storage at cryogenic temperatures (i.e., 20 K), and solid-state hydrogen storage like metal hydrides (MHs), which offer the advantage of safely storing hydrogen at a moderate temperature and pressure compared to other storage technologies (i.e., gaseous and liquid storage) (Sakintuna et al., 2007). The main problem that keeps MH reactors from being widely used, though, is how to best handle the heat during the exothermic absorption and endothermic desorption processes.

Many attempts have been made to increase the hydrogen charging rate by improving heat transfer, such as the addition of cooling tubes, fins, aluminum foam, and expanded graphite. Kikkinides et al. (Kikkinides et al., 2006) developed a 2D mathematical model to address the optimal design and operation of hydrogen storage in $LaNi_5$ MH systems. Through optimisation, the storage time might be increased by 60%. Ferekh et al. (Ferekh et al., 2015) conducted a comparative study in Zr-Co hydride beds using a heat fin and Al-foam. They demonstrated that the MH design with Al-Foam outperformed the MH design with heat fins. Darzi et al. (Darzi et al., 2016) used an annular jacket filled with phase change material (PCM) around a tubular MH reactor containing $LaNi_5$ alloy. They found that the improvement in thermal conductivity of PCM by adding Al-foam significantly enhanced the performance of the MH reactor.

For heat extraction, MH systems typically use traditional HTFs like water, oil, and air. Water can operate at low temperatures; however, for high temperatures, air or oils were used (Kukkapalli et al., 2023). Furthermore, due to their low thermal conductivity, conventional HTFs have reached their limit in terms of enhancing heat transfer performance (Humaira et al., 2023). The increasing thermal conductivity of the fluids can passively enhance heat transfer. The addition of nanoparticles (with a size less than 100 nm) to conventional HTFs increases the thermal conductivity of the mixture, thereby improving the thermal capacity of the base fluid (Wang, 2007 et al.; Tao et al., 2023). However, heat transfer augmentation comes with the penalty of a higher pressure drop. When the concentration of nanoparticles increases, the viscosity of the nanofluid (NF) also rises; consequently, it provides significantly greater pumping power compared to the base fluid.

Recently, NF has demonstrated exceptional heat diffusion capabilities and has emerged as a feasible alternative to traditional coolants in MH systems such as air, oil, or water. In the $MmNi_{4.6}Al_{0.4}$ MH reactor, Urunkar and Patil (Urunkar and Patil, 2021) used a variety of nanofluids as cooling fluids. They showed that the CuO/H_2O nanofluid enhanced the thermal transfer rate of the MH reactor by a maximum of 10% and reduced the filling duration by 9.5%. According to Elarem et al. (Elarem et al., 2021) the reactor with nano-enhanced and nanofluid improves storage time by 33.5%. Kanti et al. (Kanti et al., 2024) employed graphene oxide (GO) nanofluid as a coolant in the $LaNi_5$ metal hydride reactor. They showed that, compared to water, the presence of GO nanofluid with a volume concentration of 1% reduced the time by 61.7%.

From the prior research studies, it was noticed that all of the works that use NFs in MH reactors for hydrogen storage focused on small-scale systems, however, thermal management on large scale MH systems still becomes a significant and challenging issue in comparison to the small-scale container, (Muthukumar et al., 2012). To the best of the authors' knowledge, no research has explored the use of NFs as HTFs in large-scale MH reactors. The primary aim of this study is to evaluate the thermal efficiency of a large-scale MH reactor containing $Ti_{0.98}Zr_{0.02}V_{0.43}Fe_{0.09}Cr_{0.05}Mn_{1.5}$ alloy using Al_2O_3/H_2O nanofluid as a coolant. This analysis will be conducted using a 3D model implemented in OpenFOAM software. The model was initially validated using numerical and experimental data acquired from existing literature sources (Ye et al., 2010 and Lin et al., 2019). Subsequently, the impact of the inlet velocity and temperature of the coolant, as well as the hydrogen supply pressure, on the MH reactor's storage performance is presented.

2. SELECTION OF NANOFLUIDs

The selection of suitable nanofluids is contingent on improving the fluid's thermophysical properties. The addition of nanoparticles to the base liquid typically leads to an increase in the thermal conductivity, density, and viscosity of the base fluid while causing a decrease in its specific heat. The rise in NF temperature leads to an increase in its thermal conductivity and heat capacity, as well as a decrease in its viscosity and density, which is advantageous for its use in MH reactors as an alternative coolant to conventional HTFs (Mosher, 2007). Historically, water has been employed as an HTF in MH systems (Kukkapalli et al., 2023). Alumina (Al_2O_3) nanoparticles are selected for their excellent thermal and chemical stability (Prakash, 2018). Thus, water-based alumina Al_2O_3 nanofluids have been selected to study the performance of the MH reactor for hydrogen storage.

3. MATHEMATICAL MODEL

3.1 Reactor geometry

The reactor considered in this study consists of a cylindrical reservoir (diameter 15 cm, height 1 m) equipped with a concentric tube, as depicted in Figure 1. The reactor contains a $Ti_{0.98}Zr_{0.02}V_{0.43}Fe_{0.09}Cr_{0.05}Mn_{1.5}$ powder alloy with a hydrogen storage capacity of 1.8 wt.% capable of storing 1 kg of H2. First, inject hydrogen is injected into the porous bed from the top area, where it absorbs through an exothermic process. The cooling fluid then convects the released heat from the reactor walls. Due to the geometrical symmetry and in order to reduce CPU calculation time, the computational domain can be reduced to one-eighth, a 45-degree section of the whole reactor (Figure 1c).

3.2 Governing equations

The model, based on the finite volume method, which comprises a set of governing partial differential equations (PDEs), is solved using the open source software OpenFOAM v7.

Because of the complexity of coupled heat and mass transport phenomena related to gas flow in porous mediums, heat transport, and absorption kinetics, the following hypotheses were made to simplify the model:

- Hydrogen in a reactor is treated as an ideal gas;
- Metal and fluid are in thermal equilibrium;
- Radiative heat transfer can be neglected;
- Thermal and physical properties are assumed to be constant.

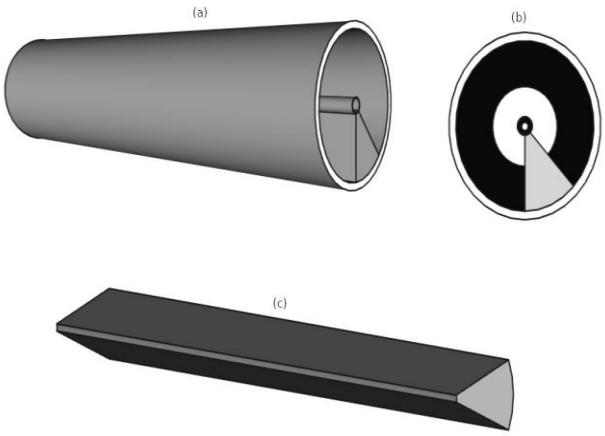

Fig 1. Schematic view of the reactor equipped with a cooling concentric tube and peripheral jacket (not to scale): (a) isometric view; (b) front view; (c) 1/8th computational domain implemented in the OpenFAOAM environment

Based on the conservation principles of mass, momentum, and thermal energy, and according to considered assumptions, the simplified coupled PDEs can be expressed as follows:

3.2.1 Mass conservation and term sources

The mass conservation in the hydride solid phase is given by (1), and in the gaseous phase inside the pores by (2):

$$\left(1-\varepsilon\right)\frac{\partial \rho_s}{\partial t} = \dot{m} \tag{1}$$

$$\varepsilon\frac{\partial \rho_g}{\partial t} + \vec{\nabla}.\left(\rho_g \vec{u}\right) = -\dot{m} \tag{2}$$

Herein, ρ_s denotes the density of metal hydride at any given time (t) during the absorption process, u being the velocity of hydrogen inside the hydride bed, and $\dot{m}$ is the hydrogen mass absorbed by the MH bed. In Eq. (2), ρ_g denotes the hydrogen density and can be obtained by the ideal gas law, which is:

$$\rho_g = \frac{PM_g}{RT} \tag{3}$$

3.2.2 Momentum conservation

Since hydrogen gas flows through a porous medium, the gas velocity is given by Darcy's law:

$$\vec{u} = \frac{K}{\mu_g}\vec{\nabla}P \tag{4}$$

Where μ_g is the dynamic viscosity of H_2 and K stands for the permeability of the porous bed calculated by the Blake-Kozeny equation:

$$K = \frac{{d_p}^2}{180} \frac{\varepsilon^3}{\left(1-\varepsilon\right)^2} \tag{5}$$

Here d_p indicates the diameter of particle. The value of μ_g is defined below:

$$\mu_g = 9.05 \times 10^{-6} \left(\frac{T}{293} \right)^{0.68} \tag{6}$$

The following equation calculates the gas pressure inside the reactor by substituting the ideal gas law (3) and Darcy's law (4) into the continuity equation (2):

$$\left(\frac{\varepsilon M_g}{RT} \right) \frac{\partial P}{\partial t} + \left(\frac{\varepsilon P M_g}{R} \right) \frac{\partial}{\partial t} \left(\frac{1}{T} \right) = \frac{K}{\mu_g} \vec{\nabla} . \left(\rho_g \vec{\nabla} P \right) - \dot{m} \tag{7}$$

3.2.3 Energy conservation

Given the assumption of thermal equilibrium between the gas and the solid, we can express a combined energy equation as follows:

$$\left(\rho c_p \right)_e \frac{\partial T}{\partial t} + \vec{\nabla} . \left(\rho_g C_{p,g} \vec{u} T \right) = \vec{\nabla} . \left(k_e \vec{\nabla} T \right) + Q_T \tag{8}$$

where, Q_T denotes the heating source, $\left(\rho c_p \right)_e$ is the effective heat capacity, and k_e is the effective thermal conductivity, which can be respectively calculated, as follow:

$$Q_T = \dot{m} \left[\Delta H + T \left(c_{p,s} - c_{p,g} \right) \right] \tag{9}$$

$$\left(\rho c_p \right)_e = \left(1-\varepsilon\right) \rho_s c_{p,s} + \varepsilon \rho_g c_{p,g} \tag{10}$$

$$k_e = \left(1-\varepsilon\right) k_s + \varepsilon k_g \tag{11}$$

where ΔH represents the enthalpy of the reaction. $c_{p,\mathrm{g}}$ and $c_{p,s}$ are the gas solid phase's specific heats, respectively. k_g , k_s denotes the thermal conductivity of the gas and solid phases, respectively. Auxiliary equations, such as the reaction kinetic equation and P-C-T relationships, are required in addition to the conservation equations previously mentioned to close the model.

3.2.4 Reaction kinetics

The amount of hydrogen absorbed by the hydride bed per unit time and per unit volume is given by the reaction rate, expressed as:

$$\dot{m} = C_a \exp\left(\frac{-E_a}{RT}\right) \ln\left(\frac{P}{P_{eq}}\right)\left(\rho_{sat} - \rho_s\right) \tag{12}$$

where C_a is a reaction-rate constant, E_a the activation energy, and ρ_s is the density of MH bed at any given time instance, ρ_{sat} is the density of saturated MH, and P_{eq} is the equilibrium pressure.

3.2.5 Thermodynamics of the reaction

The P-C-T formulations are required to describe the relationship between pressure, hydrogen concentration, and temperature. The modified Van't-Hoff relationship is used to compute the equilibrium pressure.

$$P_{eq} = f(\mathrm{H/M}) \exp\left[\left(\frac{\Delta H}{R}\right)\left(\frac{1}{T} - \frac{1}{T_{ref}}\right)\right] \tag{13}$$

where ΔH is the reaction enthalpy, R is the ideal gas constant, T_{ref} is the reference temperature, and $\mathrm{H/M}$ denotes the absorbed hydrogen to metal atomic ratio.

3.2.6 Initial and boundary conditions

Initially, the metal hydride bed is in the thermodynamic equilibrium state:

$$\rho = \rho_0 \,;\; T = T_0 \tag{14}$$

For boundary conditions, the tank walls are assumed to be impermeable and no-slip velocity. The boundary condition at the inlet can be expressed as:

$$\rho = \rho_i \,;\; T = T_i \tag{15}$$

Furthermore, the adiabatic walls can be set as,

$$\frac{\partial T}{\partial r} = 0 \tag{16}$$

As the heat generated is removed from the reactor, convective boundary conditions allow us to write:

$$-k_w \frac{\partial T}{\partial r} = h_{ext}\left(T - T_f\right) \tag{17}$$

3.3 Thermophysical properties of nanofluid

The thermo-physical properties of NPs and NFs for different concentrations are listed in Table 1. The density, thermal conductivity, specific heat capacity, and viscosity of the Al_2O_3/H_2O nanofluid are calculated using the following equations (Mohammed et al.; 2010, Einstein et al., 1956; Maxwell, 1873).

$$\rho_{nf} = (1-\varphi)\rho_{bf} + \varphi\rho_{np} \tag{18}$$

$$(\rho c_p)_{nf} = (1-\varphi)(\rho c_p)_{bf} + \varphi(\rho c_p)_{np} \quad (19)$$

$$k_{nf} = \frac{k_{np} + 2k_{bf} + 2(k_{np} - k_{bf})\varphi}{k_{np} + 2k_{bf} - (k_{np} - k_{bf})\varphi} \quad (20)$$

$$\mu_{nf} = (1 + 7.3\varphi + 123\varphi^2)\mu_{bf} \quad (21)$$

Where φ is particle volume fraction, the subscript **nf** refers to nanofluid, **bf** refers to base fluid, and **np** refers to nanoparticle.

Table 1. Water and alumina nanofluid thermal-physical properties.

Properties	Base fluid (water)	Al_2O_3/H_2O (φ =5%)
Density (kg/m3)	998.2	1148.3
Specific heat (J/kg-K)	4180	3607
Thermal conductivity (W/m-K)	0.613	0.69
Viscosity (N/m-s)	0.001003	0.001679

3.4 Numerical solution procedure

The numerical model described above was implemented in OpenFOAM using the pre-existing icoFoam solver available in the OpenFOAM toolkit. IcoFoam is a transient solver for incompressible laminar flow uses the PISO (Pressure-Implicit with Splitting of Operators) algorithm, which is based on finite volume method (FVM) to solve the pressure-velocity coupling equation. The flowchart of the PISO algorithm is shown in Figure 2. The implicit Euler method was employed for transitory time, whereas the second-order upwind technique was utilized for other transport parameters. The icoFoam solver was modified to model fluid flow in porous media by incorporating Darcy's factor into the momentum equation. A heat-transport equation with a customized convective boundary condition was also added to the solver. The convergence criteria, with a residual of 10^{-8} were set for all variables.

3.5 Grid dependence

The influence of grid sizes on the results was conducted with different grid sizes, ranging from coarse to finer. Figure 3, which presents the comparative distribution of the averaged bed temperature. The grid independence check was performed using the utility blockMesh existing in OpenFOAM. The plot shows that the simulation results are independent of mesh size for most of the domain between normal and finer meshes. Hence, the normal grid size has been chosen for further simulations in the current study.

3.6 Model validation

In order to verify the precision of the aforementioned numerical model, measured and numerical data from 26 and 27 were used as reference to verify our model. The temperature is located at X=6 mm and Z=70 mm were tested under supply pressure and cooling temperature of 1 Mpa and 290 K, respectively. There is a satisfactory correspondence between the model and experimental data as well as numerical results as can be observed in Figure 4, which confirmed the accuracy of our models.

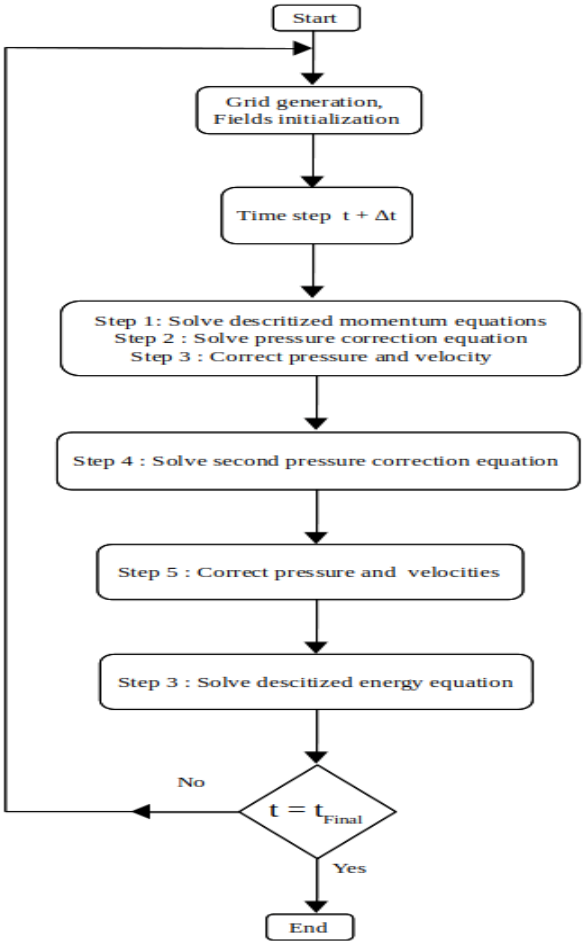

Fig 2. Flowchart of the PISO algorithm (Versteeg HK, 2007)

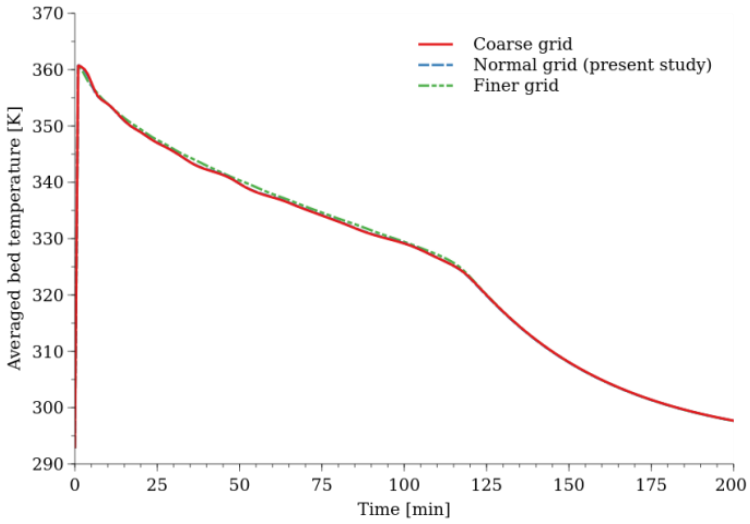

Fig 3. Grid independence test

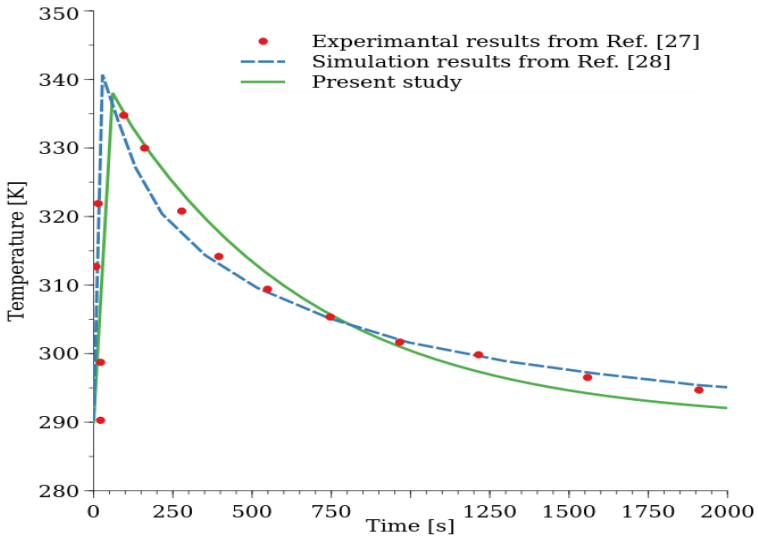

Fig 4. Simulation results versus experimental data

4 RESULTS AND DISCUSSION

The following analysis aims to examine numerically the influence of coolants, including water and water-based nanofluid, on the storage performance of a large-scale Ti-Mn-based MH reactor.

4.1 Impact of adding Al_2O_3 nanoparticles into pure water on average bed temperature and reacted fraction

Figure 5 compares the time evolution of average bed temperature and the reacted fraction of Al_2O_3/H_2O nanofluid with a volume concentration of 5% and pure water at a coolant flow velocity of 0.1 m/s. Compared to pure water, the findings demonstrated that Al_2O_3/H_2O nanofluid with 5 vol% exhibits enhanced heat transfer performance. The addition of Al_2O_3/H_2O nanoparticles to the base fluid (water) improves its thermal properties compared to pure water, resulting in an accelerated rate of heat transfer and a decrease in the average bed temperature. The Al_2O_3/H_2O nanofluid can improve heat transfer for the MH reactor by approximately 11.5%. This, in turn, reduces the time required to reach 90% storage by 18.1%, as depicted in Figure 6.

4.2 Impact of HTF fluid flow velocity

To examine the effect of the coolant flow velocity on heat transfer performance in the MH reactor, the flow velocity of Al_2O_3/H_2O nanofluid with 5 vol% was varied at 0.01, 0.05, 0.1, 0.1, and 1 m/s. Figure 7 illustrates that the velocity of the nanofluid beyond 0.1 m/s has a minimal impact on heat transfer. The observed outcome can be explained by the bed's poor thermal conductivity, which negatively affects heat diffusion.

4.3 Dependence of hydrogen charging time on hydrogen supply pressure with Al_2O_3/H_2O nanofluid and pure water

It is found that the duration required to reach maximum storage capacity reduces as the supply pressure increases. The dependence of charging time on the hydrogen supply pressure with Al_2O_3/H_2O nanofluid at 5 vol% and pure water is illustrated in Figure 8. In this study, it is seen that the 90% saturation time decreases as the hydrogen supply pressure increases for both Al_2O_3/H_2O nanofluid and pure water. Also,

the 90% saturation time of Al_2O_3/H_2O nanofluid is significantly shorter than that of water, owing to the important variation between hydrogen supply pressure and the temperature of the MH bed.

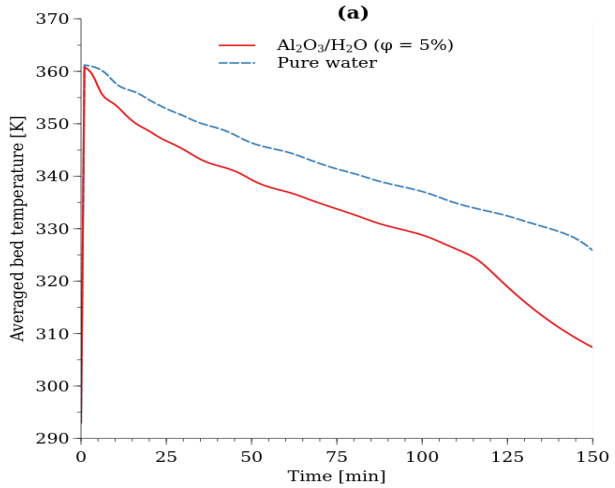

Fig 5. Time histories of averaged bed temperature and reacted fraction

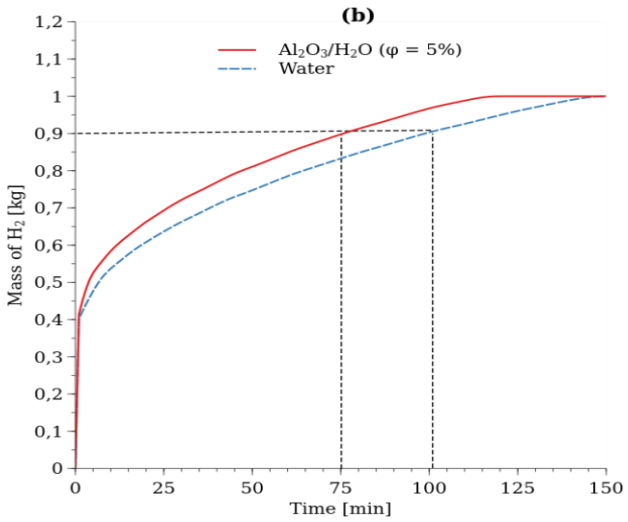

Fig 6. Time histories of absorbed hydrogen

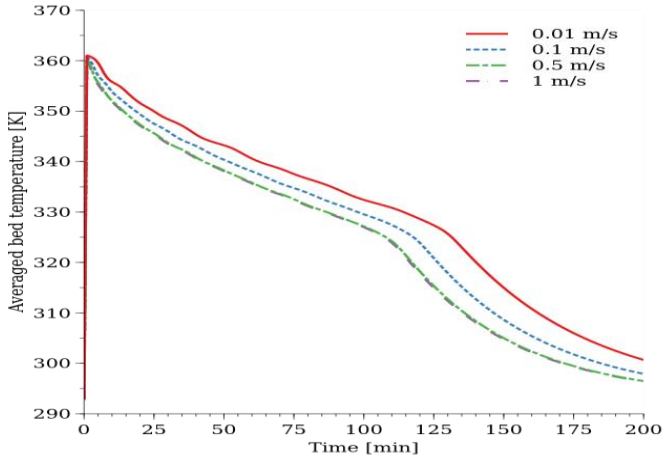

Fig 7. Time histories of averaged bed temperature with various fluid flow velocities

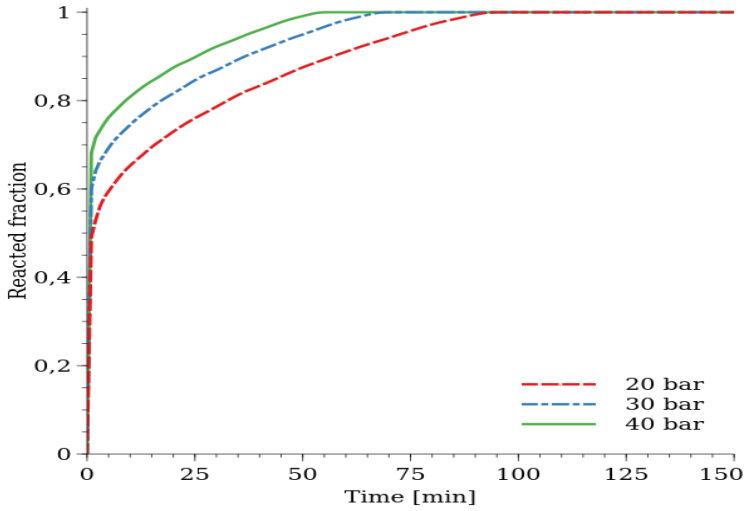

Fig 8. Effect of hydrogen supply pressure of Al_2O_3/H_2O and water on reacted fraction

4.4 Dependence of hydrogen charging time on the inlet temperature of nanofluid

In order to examine the effect of the Al_2O_3/H_2O nanofluid inlet temperature on the rate of the hydrogen charging process, the inlet temperature was varied to 293, 298, and 313 K. Figure 9 shows that lower coolant inlet temperatures lead to a decrease in hydrogen charging time. However, a rise in temperature causes an increase in the equilibrium pressure, thereby impeding the process of hydrogen charging (Eqs. (12) and (13)).

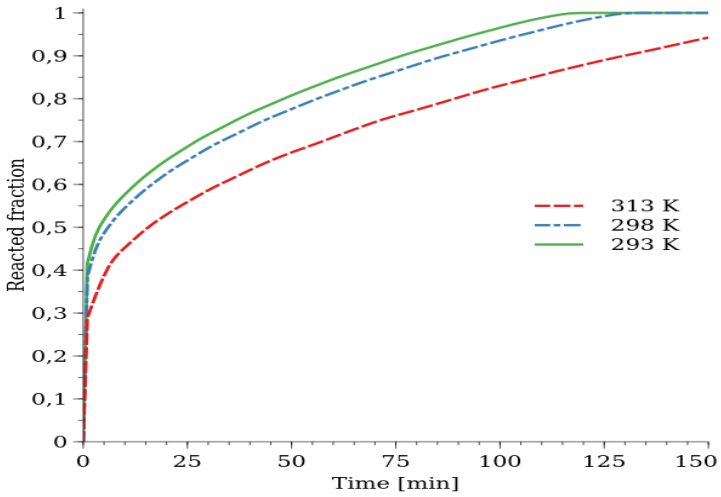

Fig 9. Effect of hydrogen supply pressure of Al_2O_3/H_2O and water on reacted fraction

4.5 Pressure drop

Figure 10 shows the pressure drop variation across different particle volume fractions with respect to flow velocity. Across all particle volume fractions tested, it is clear that the pressure drop rises exponentially with higher velocity rates. Adding Al_2O_3 nanoparticles to the base fluid makes the Al_2O_3/H_2O nanofluid thicker, which makes the frictional forces inside the cooling device stronger. As flow velocities decrease, the pressure difference between the Al_2O_3/H_2O nanofluid containing 5 vol% and pure water decreases. However, increased flow velocities result in a significant difference in the pressure drop. It is observed that the pressure drop across the MH reactor is a little greater than that in pure water.

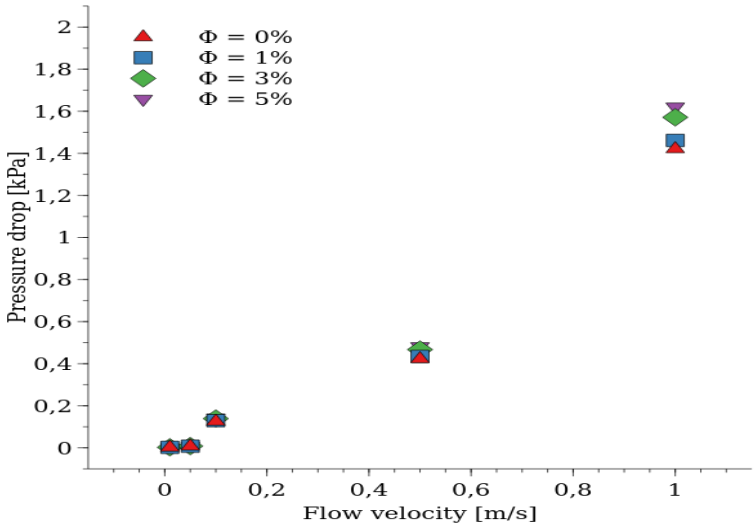

Fig 10. Pressure drop for various nanoparticles volume concentrations

5. CONCLUSION

This study developed a 3D computational model using the open-source CFD software "OpenFOAM" to evaluate the rates of heat and mass transfer in a large-scale titanium-manganese (Ti-Mn) MH reactor. The impact of the inlet coolant velocity, temperature, and hydrogen supply pressure, on the storage performance of the MH rector was examined. Some conclusions can be drawn from the present results. The nanofluid coolant, consisting of Al_2O_3/H_2O at 5 vol%, exhibits enhanced thermal efficiency in comparison to pure water. It can increase the rate of heat transfer by 11.5% and 18.1% enhancement of the time needed for 90% storage. Decreasing the nanofluid's inlet temperature can greatly accelerate the process of extracting heat from the reactor, resulting in a decrease in hydrogen charging time. A noticeable effect was detected when the flow velocities of the coolant increased, while this effect was insignificant at high flow velocities. The pressure drop across the MH reactor is just slightly greater than that in pure water. Large-scale MH systems can effectively use nanofluid as an alternative cooling fluid.

REFERENCES

Ahmad, H., Kamarudin, S. K., Minggu, L. J., & Kassim, M. (2015). Hydrogen from photo-catalytic water splitting process: A review. Renewable and Sustainable Energy Reviews, 43, 599-610.

Darzi, A. A. R., Afrouzi, H. H., Moshfegh, A., & Farhadi, M. (2016). Absorption and desorption of hydrogen in long metal hydride tank equipped with phase change material jacket. international journal of hydrogen energy, 41(22), 9595-9610.

Demirel Y. Energy: production, conversion, storage, conservation, and coupling. Springer Science & Business Media, 2012.

Einstein, A. (1956). Investigations on the Theory of the Brownian Movement. Courier Corporation.

Elarem, R., Alqahtani, T., Mellouli, S., Edacherian, A., Askri, F., & Jemni, A. (2021). Numerical analysis of a built-in thermal storage system of metal hydride and nanoparticles enhanced phase change material and nanofluid. International Journal of Energy Research, 45(4), 5881-5893.

Ferekh, S., Gwak, G., Kyoung, S., Kang, H. G., Chang, M. H., Yun, S. H., ... & Ju, H. (2015). Numerical comparison of heat-fin-and metal-foam-based hydrogen storage beds during hydrogen charging process. International Journal of Hydrogen Energy, 40(42), 14540-14550.

Kanti, P. K., Shrivastav, A. P., Sharma, P., & Maiya, M. P. (2024). Thermal performance enhancement of metal hydride reactor for hydrogen storage with graphene oxide nanofluid: model prediction with machine learning. International Journal of Hydrogen Energy, 52, 470-484.

Kikkinides, E. S., Georgiadis, M. C., & Stubos, A. K. (2006). On the optimization of hydrogen storage in metal hydride beds. International Journal of Hydrogen Energy, 31(6), 737-751.

Kukkapalli, V. K., Kim, S., & Thomas, S. A. (2023). Thermal management techniques in metal hydrides for hydrogen storage applications: a review. Energies, 16(8), 3444.

Lin, X., Sun, D., Chen, S., Zhu, Q., Leng, H., & Li, Q. (2019). Numerical analysis on pulverization and self-densification for hydrogen storage performance of a metal hydride tank. Applied Thermal Engineering, 161, 114129.

Maxwell, J. C. (1873). A treatise on electricity and magnetism (Vol. 1). Clarendon press.

Mazzucco, A., Dornheim, M., Sloth, M., Jensen, T. R., Jensen, J. O., & Rokni, M. (2014). Bed geometries, fueling strategies and optimization of heat exchanger designs in metal hydride storage systems for automotive applications: A review. International Journal of Hydrogen Energy, 39(30), 17054-17074.

Mohammed, H. A., Gunnasegaran, P., & Shuaib, N. H. (2010). Heat transfer in rectangular microchannels heat sink using nanofluids. International Communications in Heat and Mass Transfer, 37(10), 1496-1503.

Mosher, D. A., Arsenault, S., Tang, X., & Anton, D. L. (2007). Design, fabrication and testing of NaAlH4 based hydrogen storage systems. Journal of Alloys and Compounds, 446, 707-712.

Msheik, M., Rodat, S., & Abanades, S. (2021). Methane cracking for hydrogen production: A review of catalytic and molten media pyrolysis. Energies, 14(11), 3107.

Muthukumar, P., Singhal, A., & Bansal, G. K. (2012). Thermal modeling and performance analysis of industrial-scale metal hydride based hydrogen storage container. International journal of hydrogen energy, 37(19), 14351-14364.

Peighambardoust, S. J., Rowshanzamir, S., & Amjadi, M. (2010). Review of the proton exchange membranes for fuel cell applications. International journal of hydrogen energy, 35(17), 9349-9384.

Qiu, L., Zhu, N., Feng, Y., Michaelides, E. E., Żyła, G., Jing, D., ... & Mahian, O. (2020). A review of recent advances in thermophysical properties at the nanoscale: From solid state to colloids. Physics Reports, 843, 1-81.

Sakintuna, B., Lamari-Darkrim, F., & Hirscher, M. (2007). Metal hydride materials for solid hydrogen storage: a review. International journal of hydrogen energy, 32(9), 1121-1140.

Suranovic, S. (2013). Fossil fuel addiction and the implications for climate change policy. *Global Environmental Change*, *23*(3), 598-608.

Taipabu, M. I., Viswanathan, K., Wu, W., Hattu, N., & Atabani, A. E. (2022). A critical review of the hydrogen production from biomass-based feedstocks: Challenge, solution, and future prospect. Process Safety and Environmental Protection, 164, 384-407.

Tanksale, A., Beltramini, J. N., & Lu, G. M. (2010). A review of catalytic hydrogen production processes from biomass. Renewable and Sustainable Energy Reviews, 14(1), 166-182.

Tao, Q., Zhong, F., Deng, Y., Wang, Y., & Su, C. (2023). A review of nanofluids as coolants for thermal management systems in fuel cell vehicles. Nanomaterials, 13(21), 2861.

Urunkar, R. U., & Patil, S. D. (2021). Enhancement of heat and mass transfer characteristics of metal hydride reactor for hydrogen storage using various nanofluids. International Journal of Hydrogen Energy, 46(37), 19486-19497.

Verhelst, S. (2014). Recent progress in the use of hydrogen as a fuel for internal combustion engines. international journal of hydrogen energy, 39(2), 1071-1085.

Versteeg HK, (2007). An introduction to computational fluid dynamics the finite volume method, 2/E. Pearson Education India.

Wang, X. Q., & Mujumdar, A. S. (2007). Heat transfer characteristics of nanofluids: a review. International journal of thermal sciences, 46(1), 1-19.

Yasmin, H., Giwa, S. O., Noor, S., & Sharifpur, M. (2023). Thermal conductivity enhancement of metal oxide nanofluids: A critical review. *Nanomaterials*, *13*(3), 597.

Ye, J., Jiang, L., Li, Z., Liu, X., Wang, S., & Li, X. (2010). Numerical analysis of heat and mass transfer during absorption of hydrogen in metal hydride based hydrogen storage tanks. International journal of hydrogen energy, 35(15), 8216-8224.